TESTS OF CONCRETE FLANGED BEAMS REINFORCED WITH CFRP BARS

By

Ashraf F. Ashour*, BSc, MSC, PhD, CEng, MIStructE

and Mohammad Family, BSc, MPhil

Ashraf F. Ashour is a senior lecturer at the School of Engineering, Design and Technology, University of Bradford, UK. His research interests include fibre reinforced composites, repair, strengthening and optimization of reinforced concrete and masonry structures.

Mohammad Family is currently working as a structural engineer at jnpgroup consulting engineers, UK. His research interests include advanced composites materials and design of concrete structures.

Keywords: Composite, Concrete, Beams, Deflection.

Total number of words: 3900

Total number of figures: 9

Total number of tables: 7

* Corresponding author, EDT1, School of Engineering, Design and Technology, University of Bradford, UK, Email.: afashour@bradford.ac.uk, Tel.:01274720582, Fax.: 01274234111.

Abstract

Tests results of three flanged and two rectangular cross-section concrete beams reinforced with carbon fibre reinforced polymer (CFRP) bars are reported. In addition, a companion concrete flanged beam reinforced with steel bars is tested for comparison purposes. The amount of CFRP reinforcement used and flange thickness were the main parameters investigated in the test specimens. One CFRP reinforced concrete rectangular beam exhibited concrete crushing failure mode, whereas the other four CFRP reinforced concrete beams failed due to tensile rupture of CFRP bars. The ACI 440 design guide for FRP reinforced concrete members underestimated the moment capacity of beams failed due to CFRP tensile rupture and reasonably predicted deflections of the beams tested.

A simplified theoretical analysis for estimating the moment capacity of concrete flanged beams reinforced with FRP bars was developed. The experimental moment capacity of the CFRP reinforced concrete beams tested compared favourably with that predicted by the theoretical analysis developed.

Introduction

Fibre reinforced polymer (FRP) composites are being used increasingly instead of steel in many applications for concrete structures such as reinforcing bars, prestressing tendons, repairing and strengthening laminates. FRP reinforcing bars have many advantages over steel reinforcement such as high tensile strength, electromagnetic neutrality, corrosion resistance and ease of handling. On the other hand, the disadvantages of FRP bars include low modulus of elasticity, low ductility and high cost compared with steel. But the ease of handling and resistance to corrosion of FRP composites are likely to reduce the labour and maintenance costs of the structure.

Although many experimental investigations [1, 4, 7-11] were conducted on FRP reinforced concrete beams with rectangular section, there has been very little research [5] into the behaviour of concrete flanged beams reinforced with FRP bars. Grace et al. [5] tested seven continuous T-section beams reinforced with different combinations of steel, CFRP and glass fibre reinforced polymer (GFRP) as longitudinal bars and stirrups. They concluded that while different FRP reinforcement arrangements were found to have the same load capacity as steel reinforcement in conventional beams, failure modes and ductility differed. The ACI guidelines for the design and construction of concrete reinforced with FRP bars [3] stated that the behaviour of reinforced concrete beams with nonrectangular cross-section has yet to be confirmed by experimental results. The main objectives of this paper are summarized below:

- To present test results of CFRP reinforced concrete beams with different cross section shapes;
- To compare the behaviour of concrete flanged beams reinforced with CFRP and steel bars;
- To compare the behaviour of CFRP reinforced concrete flanged and rectangular concrete beams;
- To examine the applicability of the ACI formulas for estimating the moment capacity and deflections of CFRP reinforced concrete flanged beams;
- To develop rational equations for estimating the moment capacity of flanged beams reinforced with FRP bars.

Test Programme

Test Specimens

The test specimens consisted of six simply supported reinforced concrete beams with an overall span of 3000mm. Five of these beams were reinforced with CFRP bars and were classified into two groups according to the cross-section shapes: 3 T-flanged beams and 2 rectangular beams, plus a steel reinforced concrete beam of a T-section for comparison purposes.

Two beams (T/C150-2 and T/C150-4) in the first group had the same geometrical dimensions but different amount of CFRP reinforcement whereas the third beam (T/C100-4) in this group was designed to have the same amount of CFRP bars as that of beam (T/C150-4) and less flange thickness as shown in Fig. 1. The flange width of 700 mm is selected to be one quarter of the beam span and the effective overhanging flange width on each side of the web is 250 mm, less than eight times the slab thickness as recommended by the ACI 318-02 [2]. The second group contained two rectangular beams (R/C-2 and R/C-4) with the same height, 350mm, as that of the T-beams T/C150-2 and T/C150-4 of the first group. Beams R/C-4 and R/C-2 had the same amount of CFRP reinforcement as beams T/C150-4 and T/C150-2, respectively, as depicted in Fig. 1. The surface of CFRP bars used in reinforcing test specimens was sand-coated.

The area of steel reinforcement used in the companion beam T/S150-3 was selected to achieve the same tensile strength as that of CFRP bars used in beam T/C150-2 based on tensile strength of CFRP and steel provided by the manufacturer. But, after the pull-out test of CFRP and steel bars, it was observed that the tensile strength of the steel bars used in beam T/S150-3 was higher than that of the CFRP bars in beam T/C150-2 and

less than that of the CFRP bars in beam T/C150-4. The three beams, T/C150-2, T/C150-4 and T/S150-3, had the same geometrical dimensions as presented in Fig. 1.

Vertical steel links of 10mm bar diameter at 100mm centres were provided throughout the shear span of the beams tested in order to prevent shear failure. All beam flanges were transversely reinforced near the top and bottom surfaces and across the full width of the flange with 8 mm diameter CFRP bars at every 200mm centres. The beam flanges were also longitudinally reinforced with one 8 mm diameter CFRP bar in each corner of the flange as illustrated in Fig. 1. Details of top and bottom reinforcements of the test specimens are also given in Table 1.

Beam Notations

The first letter of the beam notation stands for the shape of the beam cross-section: T for flanged cross sections and R for rectangular cross-sections. The second letter identifies the type of longitudinal bottom reinforcement: 'C' for CFRP bars and 'S' for steel bars. In flanged beams, the first number indicates the beam flange thickness in millimetres i.e. 100mm or 150mm and the second number gives the number of bottom reinforcing bars i.e. 2, 3 or 4. The number in the rectangular beam notation gives the number of bottom reinforcing bars. For example a beam notation T/C150-2 means that this beam had a T-flange of 150mm thickness and reinforced with 2 CFRP bottom bars.

Material Properties

Casting of all six beams took place in two phases. Group T/C beams were cast first using a ready mixed concrete batch of a target compressive strength of 35 N/mm^2 at 28 days. Group R/C and the companion steel beam T/S150-3 were cast from a second ready mixed concrete batch of the same target compressive strength as group T/C. For each phase, eighteen 100 mm cubes, eight 150 mm diameter ×300 mm high cylinders and three 100×100×500 mm prisms were made. All test specimens were demoulded

after 24hrs, wet cured and covered with polyethylene sheets until the date of testing. The cubes, cylinders and prisms were tested immediately after testing of the corresponding beam to provide values for the cube compressive strength, f_{cu}, the splitting tensile strength, f_t, and the modulus of rupture, f_r, respectively. The average results of cube, cylinder and prism tests are given in Table 1.

The mechanical properties of steel reinforcing bars used in the test beams as stirrups and in the companion steel beam T/S150-3 as longitudinal reinforcing bars were obtained by carrying out uniaxial tensile tests on three steel bar specimens. Table 2 gives the yield strength, ultimate tensile strength, and modulus of elasticity, obtained for different diameters of steel bars used.

Since mechanical damage can occur due to surface serrations of traditional wedge-shaped grips, CFRP bars cannot be tested using the same gripping technique as that used for steel. Hence, it was necessary to encase the ends of CFRP specimens in an anchorage system to distribute the grip stresses so they were not concentrated on critical points of CFRP bars. A tubular anchorage system made of steel pipes filled with expanding glue filler is used to anchor the two ends of CFRP bars. Any premature failure due to bond slippage of the bar from the steel pipe is rejected. Table 2 presents the average tensile strength, and modulus of elasticity, of three specimens of CFRP bars that were successfully tested for each bar diameter using the above mentioned end anchorage.

Test Set-up and Instrumentation

Each test beam contained one span supported on one end roller and one end hinge supports. The test specimen was symmetrically loaded by two concentrated point loads at the same distance of 350 mm from the beam mid-span, as shown in Fig. 1, via a hydraulic ram and an independent steel reaction frame, which was bolted to the strong

floor of the laboratory. Beam deflections were measured using dial gauges at 5 points: at mid-shear spans, under each point load and at mid-span as shown in Fig. 1.

Test Results and Discussion

The total load (sum of the two point loads) was applied in small load increments. After each load increment, any cracks were marked on the beam surface with an indelible marker to trace the crack propagation. Any distinct behaviour noticed during testing such as noise emission was recorded. Beam failure was judged to occur when the beam under testing could not sustain any more additional load. Immediately after the beam failure, the applied load was released and no further data were recorded.

Crack Patterns

Before loading of each beam the surface of the beam was white-painted to ease marking of cracks during the testing. First crack in Group T/C beams appeared vertically in the beam flexural zone between 22 and 35 kN. First crack in beam T/C150-4 occurred at 35 kN whereas that in beam T/C150-2 and T/C100-4 appeared after applying 22 kN. In the second group beams, the first flexural crack in beams R/C-2 and R/C-4 appeared at 22 kN. The first flexural crack in the companion steel reinforced concrete beam T/S150-3 appeared at 35 kN total applied load. Table 1 presents the loads at which each beam experienced its first crack. Overall, the flange thickness and amount of reinforcement had a small effect on the first cracking load of the beams tested.

As the load was increased, more cracks occurred within the flexural zone of each beam and existing cracks propagated perpendicular to the direction of principal tensile stresses along the beam length. Cracks in the CFRP reinforced concrete beams were more visible and recognizable than that of the companion steel reinforced concrete beam T/S150-3 where the first few cracks were hardly visible. Even in some cases, such

as in beam T/C150-4, the first few cracks occurred with a little sound. This could be attributed to the bond-slip between CFRP bars and concrete. Overall, flanged beams exhibited more cracks than beams with rectangular section, both reinforced with CFRP bars.

Failure Modes

Three different modes of failure were observed in the tests and are described below.

Mode 1 Conventional ductile flexural failure: This mode of failure was observed for the companion steel beam T/S150-3, due to yielding of the bottom steel reinforcement at mid-span section followed by concrete crushing, as shown in Fig. 2.

Mode 2 concrete crushing: Beam RC-4 exhibited this mode of failure. Failure occurred by crushing of concrete in the compression zone as the beam was over-reinforced. After the beam failure by concrete crushing, more loads were applied to the beam and shortly after the bottom CFRP reinforcement failed in rupture with a loud sound (Fig. 3).

Mode 3 CFRP rupture: The other four beams failed by sudden and catastrophic rupture of the tensile bottom CFRP reinforcement. This failure mode was noticed in beams T/C150-2 (Fig. 4), T/C150-4, T/C100-4 and R/C-2. All reinforcement rupture occurred under the applied point load. The beam failure was accompanied by loud sound, wide cracks and excessive deflections. Rupture of the CFRP bars observed after beam failure was not as visible as typical GFRP bar rupture presented in previous experimental tests [1, 8] but it appeared as minuscule cracks along the bar length.

Load Capacity

Table 1 presents failure loads along with failure modes of the beams tested. The results show that the highest failure load of 277.5 kN in T-beams reinforced with CFRP bars was experienced by beam T/C150-4, whereas beam T/C100-4 with the same amount of reinforcement but less flange thickness and overall depth failed at a lower load of 199.3

kN. Flanged beams exhibited a higher failure load than rectangular beams of the same depth and amount of CFRP reinforcement. Rectangular beam R/C-4 which had the same depth as beam T/C150-2 but double the amount of CFRP reinforcement failed at a much higher load. This is mainly attributed to the efficient use of the compression zone of concrete as beam R/C-4 failed in concrete crushing whereas beam T/C150-2 failed in FRP bar rupture. Overall, the existence of the flange increased the beam load capacity; however this effect would be higher if beams would have failed due to concrete crushing.

Beam Deflections

Fig. 5 shows the relationship between the total applied load and the mid-span deflection of all test specimens. At early stages of loading before the onset of concrete cracking, beams T/C150-2, T/C100-4, R/C-2 and R/C-4 exhibited fairly similar stiffness, where as beams T/C150-4 and T/S150-3 were slightly stiffer. After cracking, there is a clear reduction in the flexural stiffness. The load levels, at which the flexural stiffness is reduced, agree well with the first cracking loads of the beams tested recorded in Table 1. After concrete cracking, beams T/C150-4 and T/S150-3 showed the highest stiffness and consequently, the smallest mid-span deflection at the same load. Beam T/C150-2 with the same dimension as beam T/C150-4 but less amount of CFRP reinforcement showed a lower stiffness and much larger mid-span deflection. Beam T/C150-4 having the same amount of reinforcement as, but thicker flange than, beam T/C100-4 exhibited higher stiffness. Although beams T/C150-2 and R/C-2 having the same depth and amount of CFRP reinforcement showed similar stiffness before the first crack, the results show higher stiffness for the flanged beam after cracking.

The companion steel reinforced concrete beam T/S150-3 showed reasonably close mid-span deflection to beam T/C150-4 in early stages of loading. But after the first crack had

appeared in concrete, the steel reinforced concrete beam T/S150-3 exhibited higher stiffness and less deflection than those of the CFRP reinforced concrete beam T/C150-4 as indicated in Fig. 5. After yielding of the bottom steel reinforcing bars (total applied loads greater than 160 kN), Beam T/S150-3 experienced the highest deflection, ductility and energy absorbed of all beams tested at failure.

Deflections of each beam were also measured at 4 other points along the beam length at each load increment. Similar conclusions to those presented above for the mid-span deflection can be drawn for other recorded deflections under the applied point loads and at mid-shear spans but figures are not presented here.

Overall, the amount of reinforcement and flange thickness does not have a major effect on the beam stiffness and deflection before the first crack, but they had a significant effect after the first crack.

Prediction of Flexural Moment Capacity of Flanged Sections

The calculation of the moment capacity of flanged sections for either concrete crushing or FRP bar rupture depends on the position of the neutral axis. There are two different situations to consider, namely when the neutral axis falls within or below the flange. If the neutral axis is within the flange thickness as shown in Fig. 6(a), then a flanged section is dealt with in exactly the same way as a rectangular section having a breadth equal to the effective width, *b*, of the flange. But, when the neutral axis lies below the flange as shown in Fig. 7(a), the flanged section is considered to be made up of two components: the overhanging flange component and the remaining web component as depicted in Fig. 7.

The estimation of the balanced reinforcement ratio ρ_{fb} is also affected by the location of the neutral axis, i.e. in the flange or web. In the following, the balanced

reinforcement ratio and moment capacity are estimated for the two flexural failure modes and for the two locations of the neutral axis.

Balanced Reinforcement Ratio

Assuming that concrete crushing ($\varepsilon_c = \varepsilon_{cu}$) and FRP rupture ($\varepsilon_f = \varepsilon_{fu}$) occur simultaneously, the neutral axis depth c_b for this case can be obtained from [3, 7, 9]:

$$c_b = \left(\frac{\varepsilon_{cu}}{\varepsilon_{cu} + \varepsilon_{fu}} \right) d \quad \text{.....(1)}$$

where ε_{fu} and ε_{cu} = rupture and crushing strains of FRP bars and concrete, respectively, ε_f and ε_c = strains in FRP bars and top fibre of concrete, respectively, and d = beam effective depth as shown in Fig. 6 or 7. The above equation (1) is independent of the location of the neutral axis, i.e. within or below the flange. The strains and force components for a balanced reinforcement case are given in Table 3, Fig. 6 and Fig. 7, assuming $\varepsilon_c = \varepsilon_{cu}$ and $\varepsilon_f = \varepsilon_{fu}$. Considering equilibrium of forces, balanced FRP reinforcement ratio $\rho_{fb} \left(= A_{fb} / bd \right)$ is given below:

$$\rho_{fb} = \frac{0.85 \beta_1 f_c^{'}}{f_{fu}} \left[\frac{\varepsilon_{cu}}{\varepsilon_{cu} + \varepsilon_{fu}} \right] \qquad \beta_1 c_b \le h_f \quad \text{.....(2)}$$

$$\rho_{fb} = \frac{0.85 f_c^{'}}{f_{fu}} \left[\frac{(b - b_w) h_f}{bd} + \beta_1 \frac{b_w}{b} \frac{\varepsilon_{cu}}{\varepsilon_{cu} + \varepsilon_{fu}} \right] \qquad \beta_1 c_b > h_f \quad \text{.....(3)}$$

where A_{fb} = area of FRP bars at balanced failure, $f_c^{'}$ = cylinder compressive strength of concrete, f_{fu} = tensile rupture of FRP bars, h_f = flange thickness, b_w = web width, b = flange width and β_1 = a cylinder compressive strength modification factor ($0.65 < \beta_1 < 0.85$) as defined in the ACI 318-02 [2] and ACI Committee 440 report [3], depending on the value of the cylinder compressive strength $f_c^{'}$ of concrete. The parameter α_1 required to define the equivalent concrete stress block in Figs. 6(c), 7(d) and 7(e) is

assumed to be 0.85 as $\varepsilon_c = \varepsilon_{cu}$. Eq. (2) or (3) gives the balanced reinforcement ratio in case of the neutral axis in the flange ($\beta_1 c_b \le h_f$) or below the flange ($\beta_1 c_b > h_f$), respectively.

Moment Capacity When Neutral Axis in Flange

Fig. 6 shows strain and stress distributions for a flanged section when the neutral axis lies in the flange. Strains, forces and equilibrium equations for flanged beams are also summarised in Table 4: Table 4(a) for concrete crushing failure mode and Table 4(b) for FRP tensile rupture failure mode. Considering strain compatibility and equilibrium of forces presented in Table 4(a), the moment capacity M_n, neutral axis depth c and FRP tensile stress f_f for concrete crushing failure mode could be estimated as given below [3]:

$$M_n = A_f f_f \left(d - \frac{\beta_1 c}{2} \right) \quad \text{.....(4)}$$

$$c = A_f f_f / \left(0.85 \beta_1 f_c^{'} b \right) \quad \le h_f / \beta_1 \quad \text{.....(5)}$$

$$f_f = \sqrt{\frac{(E_f \varepsilon_{cu})^2}{4} + \frac{0.85 \beta_1 f_c^{'}}{\rho_f} E_f \varepsilon_{cu}} - 0.5 E_f \varepsilon_{cu} \le f_{fu} \quad \text{.....(6)}$$

where A_f = area of FRP bars, E_f = modulus of elasticity of FRP bars.

In case of FRP rupture mode of flexural failure, the crushing concrete strain ε_{cu} may not be attained. Therefore, the two parameters α_1 and β_1 required to approximate the equivalent rectangular stress block of concrete in compression depend on the particular strain level reached. The values of α_1 and β_1 for a specified strain ε_c at the extreme compression fibre and the cylinder compressive strength $f_c^{'}$ of concrete are derived in reference [6]. A trial and error approach is adopted to estimate the depth of the neutral axis that satisfies the linear strain distribution and equilibrium of forces as defined in

Table 4(b) and Fig. 6. The moment capacity is then estimated using the moment equilibrium equation given in Table 4(b).

In order to overcome the complexity of the iterative process mentioned above, ACI committee 440 [3] suggested the use of an approximate but conservative formula for estimating the moment capacity M_n in case of FRP bar rupture as given below:

$$M_n = A_f f_{fu}\left(d - \frac{\beta_1 c_b}{2}\right) \quad \text{.....(7)}$$

where c_b = neutral axis depth in case of balanced failure as defined by Eq. (1). The above analysis is valid as long as the neutral axis depth c lies in the flange, i.e. $c \le h_f / \beta_1$. This is likely to occur for under reinforced beams ($\rho_f \le \rho_{fb}$).

Moment Capacity When Neutral Axis below Flange

When the neutral axis lies below the flange as shown in Fig. 7(a), Eq. (4) or (7) cannot be used to calculate the moment capacity and the analysis separately considers the resistance provided by the overhanging flanges (Fig. 7(d)) and that provided by the remaining rectangular part (Fig. 7(e)). Table 5 identifies strains, forces, moments and equilibrium equations when the neutral axis falls below the flange: Table 5(a) for concrete crushing failure mode and Table 5(b) for FRP tensile rupture failure mode based on the distribution of strains and stresses given in Figs. 7(d) and (e), respectively. To estimate the position of the neutral axis c for either concrete crushing or tensile rupture failure mode, an iterative procedure is adopted to satisfy the strain compatibility and force equilibrium equations stated in Table 5. The moment capacity M_n is then calculated by taking moments of forces about the level of FRP bars as given in Table 5(a) for concrete crushing failure mode and Table 5(b) for FRP tensile rupture.

Table 6 presents the estimated values of different parameters from the above theoretical analysis. In all the three flanged beams, the estimated neutral axis depth was less than

the flange thickness. All the three flanged beams, T/C150-2, T/C150-4 and T/C100-4, were identified as under reinforced and failed due to tensile rupture of CFRP bars as observed in the tests. The predicted failure modes of the other two rectangular beams also agree with those observed in experiments. Table 6 indicates that the balanced area of CFRP reinforcement of flanged beams is much higher than that of rectangular beams. Fig. 8 compares the flexural moment capacity measured in the current tests against those obtained from the theoretical analysis presented above and the formula proposed by ACI committee 440 [3]. Figure 8 and Table 6 illustrate that the theoretical method reasonably predicted the moment capacity of the test specimens. The ACI committee 440 predictions were conservative for the case of tensile rupture of CFRP bars. For concrete crushing failure mode, both the ACI committee 440 and current theoretical analysis predictions were close to the experimental moment capacity of beam R/C-4.

Prediction of Deflections

Most of the formulas [1, 3, 4, 7-10] proposed to estimate the deflection of FRP reinforced concrete beams after cracking were developed by modifying the Branson formula used for steel reinforced concrete beams. For example, ACI committee 440 [3] suggested the following expression for the effective moment of inertia, I_e:

$$I_e = \left(\frac{M_{cr}}{M_a}\right)^3 \beta_d I_g + \left(1 - \left(\frac{M_{cr}}{M_a}\right)^3\right) I_{cr} \qquad \leq I_g \quad \text{.....(8)}$$

where

$$\beta_d = \alpha_b \left(\frac{E_f}{E_s} + 1\right) \text{.....(9)}$$

where I_g = the gross moment of inertia, I_{cr} = the transformed cracked moment of inertia calculated using an elastic analysis, M_a and M_{cr} = applied and cracking moments, respectively, E_f and E_s = elastic modules of FRP and steel bars, respectively, and α_b = a

bond-dependent coefficient. The reduction parameter β_b defined by Eq. (9) is introduced to account for the difference in the modulus of elasticity and bond characteristics of FRP and steel bars. The above equation (8) is only valid for $M_a > M_{cr}$, but for $M_a < M_{cr}$, the gross moment of inertia I_g should be used. Different researchers [1, 3, 4, 7-11] evaluated Eq. (8) and consequently suggested different values for α_b or β_b parameter to achieve good correlations with experimentally measured deflections as summarised in Table 7. The mid-span deflection Δ for a simply supported beam subjected to two equal point loads is given by the following equation:

$$\Delta = \left(3L^2 - 4a^2\right)\frac{Pa}{24 I_e E_c} \quad \text{.....(10)}$$

where L = the span of the beam, a = shear span, E_c = concrete elastic modulus and P = total applied load at which deflection is calculated. Figure 9 compares the experimental mid-span deflection of the CFRP concrete beams tested and the theoretical predictions obtained from Eqs. (8), (9) and (10) with different values of α_b or β_b for different applied moments. Figure 9 shows that the predicted first cracking loads, where the flexural stiffness is clearly reduced, reasonably agree with those observed in experiments for all beams tested but beam T/C150-2. In addition, the flexural rigidity before cracking was closely predicted for all beams tested. Figure 9 illustrates that the less the value of β_b, the less the predicted beam stiffness after cracking. The values of β_b between 0.5 and 1 do not have a significant effect on the predicted deflection, especially for beams with higher amount of CFRP reinforcement (Beams T/C150-4, T/C100-4 and R/C-4). For values of β_b = 0.2, the flexural stiffness was quickly softened after cracking but the effect of β_b on the predicted deflection is decreased as the applied moment, M_a, is increased. Apart from beam T/C150-4, there is a good agreement between the

experimental and predicted mid-span deflections after cracking for different values of β_b proposed in the literature.

Conclusions

Test results of 6 simply supported reinforced concrete beams, including three flanged and two rectangular CFRP reinforced concrete beams and a companion steel reinforced concrete beam with flanged cross-section are presented. The experimental results for the moment capacity and deflections are compared with the equations proposed by ACI 440 committee. Based on strain compatibility and equilibrium equations, a theoretical analysis for the prediction of the moment capacity when the neutral axis lies within or below the beam flange was developed. The principal findings of the research presented in this paper are summarised below:

- Crack width in CFRP reinforced concrete flanged beams was greater than that of the companion steel reinforced concrete flanged beam.
- The amount and type of reinforcement had a considerable effect on the beam stiffness and deflection after the occurrence of the first crack.
- Flanged beams showed stiffer behavior and higher load capacity than rectangular beams with the same amount of CFRP reinforcement and depth.
- All flanged beams failed due to CFRP tensile rupture, however, their load capacity has increased compared with rectangular beams with the same amount of CFRP reinforcement. This mode of failure was brittle and accompanied with loud sound, wide cracks and excessive deflections.
- The ACI 440 formula for the calculation of the moment capacity of CFRP reinforced concrete beams gives conservative prediction compared with experiments. It needs, however, to be further developed to account for the case when the neutral axis falls below the flange.

- The ACI 440 method for the calculation of deflections of FRP reinforced concrete beams reasonably predicted the deflection of the flanged beams tested.
- The load capacity of the beams tested compared well with those predicted by the theoretical analysis.

Reference

1. Abdalla, H. A., (2002), "Evaluation of Deflection in Concrete Members Reinforced with Fibre Reinforced Polymer (FRP) Bars," Composites Structures, Vol. 56, pp. 63-71.

2. ACI Committee 318 (2002), "Building Code Requirements for Structural Concrete (ACI 318-02) and Commentary (318R-02)," American Concrete Institute, Farmington Hills, Mich., 443p.

3. ACI committee 440 (2001), "Guide for Design and Construction of Concrete Reinforced with FRP Bars (ACI 440.1R-01)," American Concrete Institute, Farmington Hills, Mich., 41p.

4. Engel, R. S., Croyle, M. G. Bakis, C. E. and Nanni, A., (1999), "Deflection of Reinforced Concrete Beams Reinforced by Fiber Reinforced Polymer Grid with Various Joint Designs," Fourth International Symposium on Fiber Reinforced polymer Reinforcement for Reinforced Concrete Structures, SP-188, C. W. Dolan, S. H. Rizkall and A. Nanni, ed., American Concrete Institute, Farmington Hills, Mich., pp. 75-85.

5. Grace, N. F., Soliman, A. K., Abdel-Sayed, G. and Saleh, K. R. (1998), "Behavior and Ductility of Simply and Continuous FRP Reinforced Beams," Journal of Composites for Construction, ASCE, Vol. 2, No. 4, pp. 186-194.

6. Hsu, T. T. C., (1993), "Unified theory of reinforced concrete," CRC press, Boca Raton, 313p.

7. Masmoudi, R., Thériault, M. and Benmokrane, B., (1998), "Flexural Behavior of Concrete Beams Reinforced with Deformed Fiber Reinforced Plastic Reinforcing Rods," ACI Structural Journal, Vol. 95, No. 6, pp. 665-676.
8. Pecce, M., Manfredi, G. and Cosenza, E. (2000), "Experimental Response and Code Models of GFRP RC Beams in Bending," Journal of Composites for Construction, ASCE, Vol. 4, No. 4, pp. 182-190.
9. Thériault, M. and Benmokrane, B., (1998), "Effects of FRP Reinforcement Ratio and Concrete Strength on Flexural Behavior of Concrete Beams," Journal of Composites for Construction, ASCE, Vol. 2, No. 1, pp. 7-16.
10. Toutnji, H. and Deng, Y. (2003), "Deflection and Crack-width Prediction of Concrete Beams Reinforced with Glass FRP Rods," Construction and Building Materials, Vol. 17, pp. 69-74.
11. Yost, J. R., Gross, S. P. and Dinehart, D. W. (2003), "Effective Moment of Inertia for Glass Fiber-Reinforced Polymers-Reinforced Concrete Beams," ACI Structural Journal, Vol. 100, No. 6, pp. 732-739.

Acknowledgement

The experimental work described in this paper was conducted in the Heavy Structures Laboratory at the University of Bradford; the assistance of the laboratory staff is acknowledged.

List of Notations

a = shear span

A_f = area of FRP bars.

A_{fb} = area of FRP bars at balanced failure.

b = flange width.

b_w = web width.

C_c = Concrete compressive resultant force – see Figs. 6 and 7.

C_f = Concrete compressive resultant force in flange – see Fig. 7.

C_w = Concrete compressive resultant force in web – see Fig. 7.

d = beam effective depth.

c_b = neutral axis depth in case of balanced failure

E_c = concrete elastic modulus

E_f = modulus of elasticity of FRP bars.

E_s = modulus of elasticity of steel.

f_{cu} = cube compressive strength of concrete.

f_c' = cylinder compressive strength of concrete.

f_f = FRP tensile stress.

f_t = splitting tensile strength of concrete.

f_r = modulus of rupture of concrete.

h_f = flange thickness.

f_{fu} = tensile strength of FRP bars.

I_{cr} = transformed cracked moment of inertia calculated using an elastic analysis

I_g = gross moment of inertia

L = span of the beam

M_a = applied moment.

M_{cr} = cracking moment.

M_n = moment capacity

P = total applied load at which deflection is calculated

T_f = Tensile force in FRP bars – see Figs. 6 and 7.

α_1 & β_1 = two parameters required to approximate the equivalent rectangular stress block of concrete in compression.

α_b = bond-dependent coefficient.

β_1 = a cylinder compressive strength modification factor ($0.65<\beta_1<0.85$).

β_b = reduction parameter to account for the difference in the modulus of elasticity and bond characteristics of FRP and steel bars.

ε_{fu} = rupture strain of FRP bars.

ε_{cu} = crushing strain of concrete.

ε_f = strain in FRP bars.

ε_c = Strain in top fibre of concrete.

Δ = mid-span deflection

ρ_{fb} = FRP balanced reinforcement ratio.

Figures and Tables

List of Figures

List of Tables

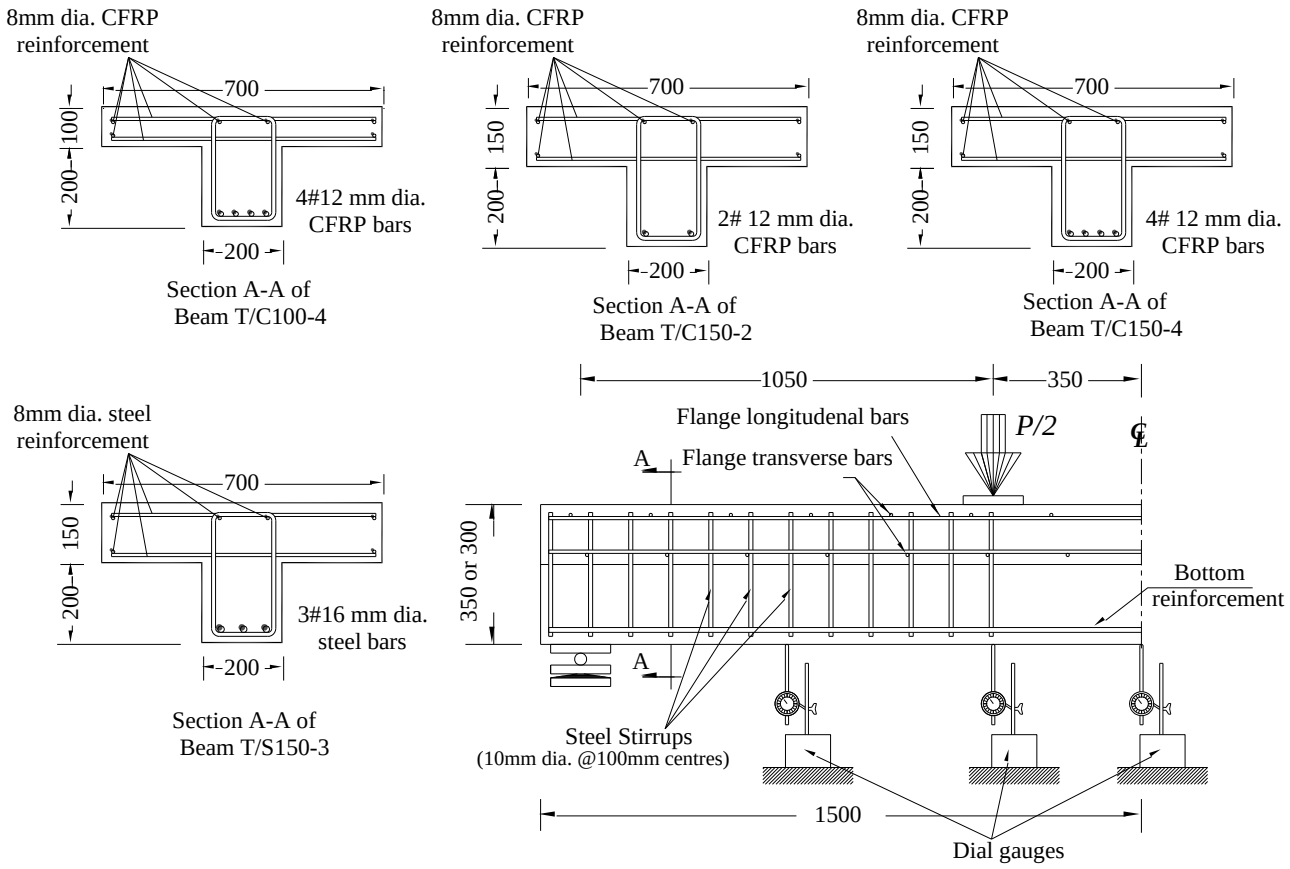

(a) Flanged Beams (T/C150-2, T/C150-4, T/C100-4 & T/S 150-3)

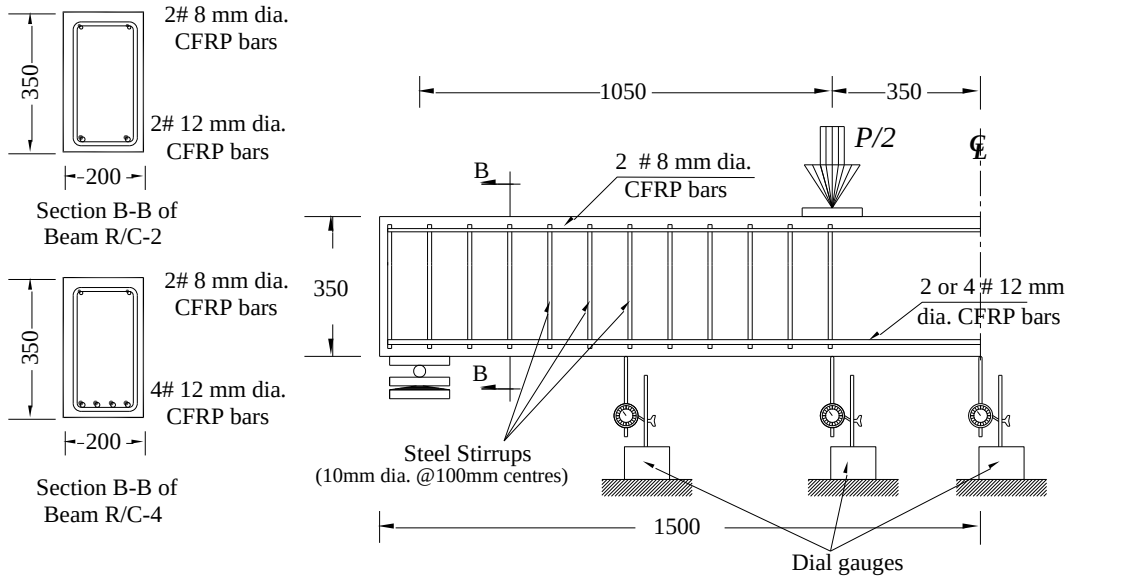

(b) Rectangular Beams (R/C-2, R/C-4)

Fig. 1: Test set up and reinforcement details of the test specimens.

(all dimensions are in mm.)

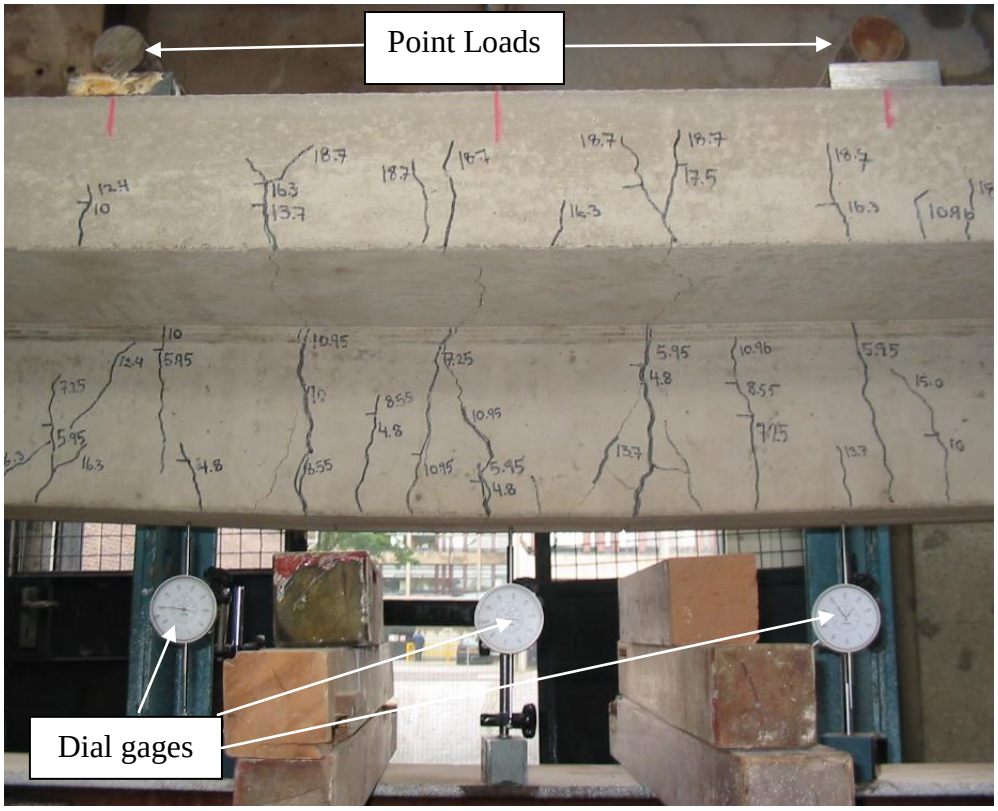

Fig. 2: Conventional flexural failure of the steel reinforced concrete beam T/S150-3.

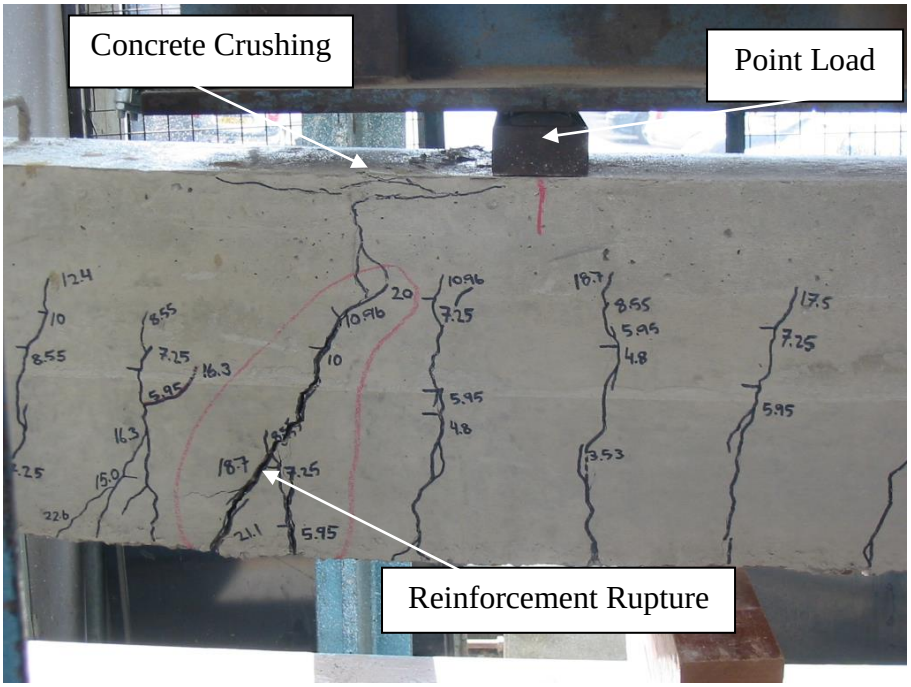

Fig. 3: Concrete crushing failure mode, followed by CFRP reinforcement rupture of Beam R/C-4.

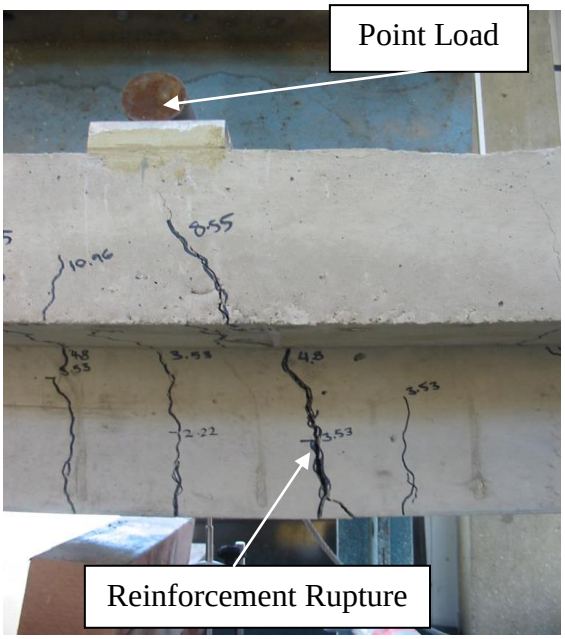

Fig. 4: Typical CFRP rupture failure mode occurred in flanged beams (T/C150-2).

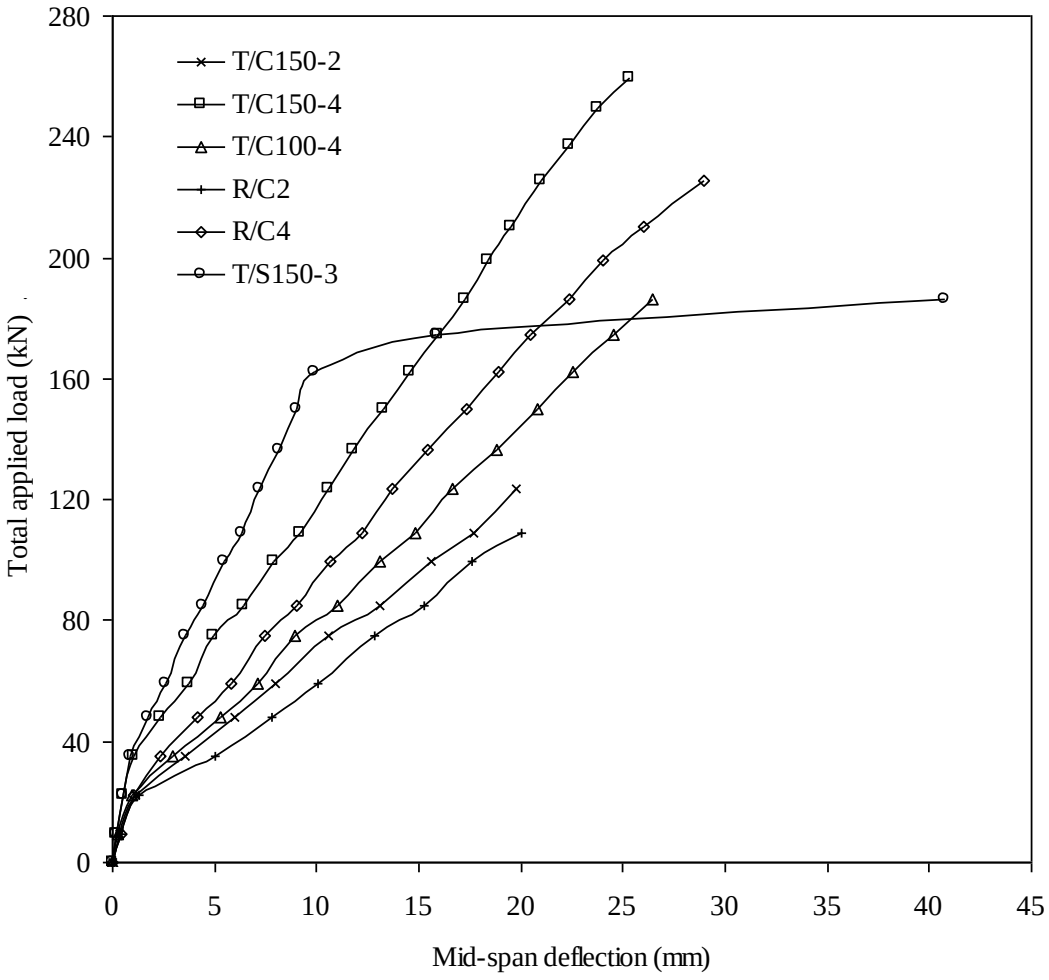

Fig. 5: Experimental mid-span deflection versus total applied load of the test specimens.

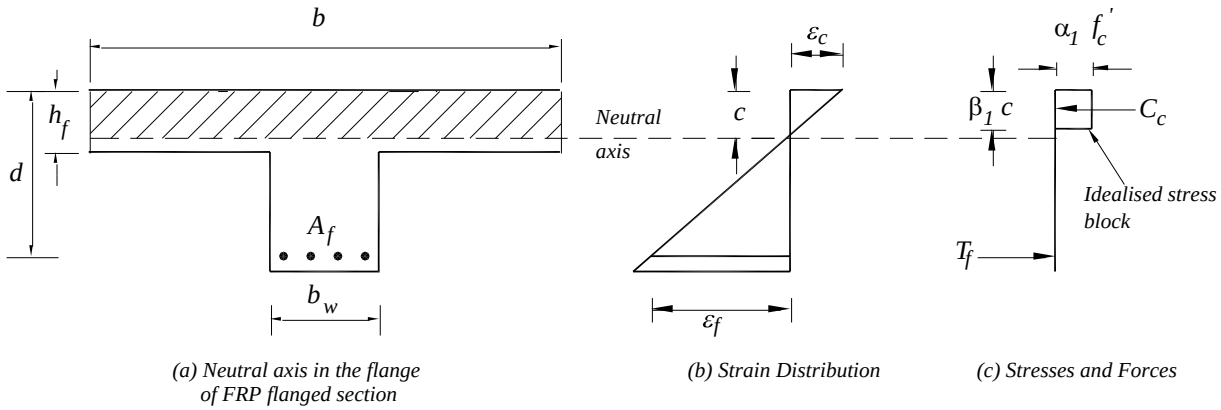

Fig. 6: Strain and stress distributions of flanged section when neutral axis in the flange.

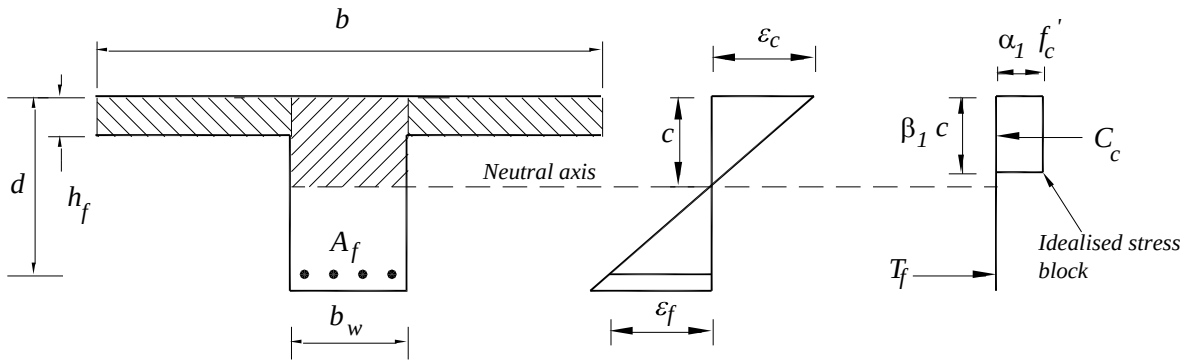

(a) Neutral axis below the flange of FRP flanged section *(b) Strain Distribution* *(c) Stresses and Forces*

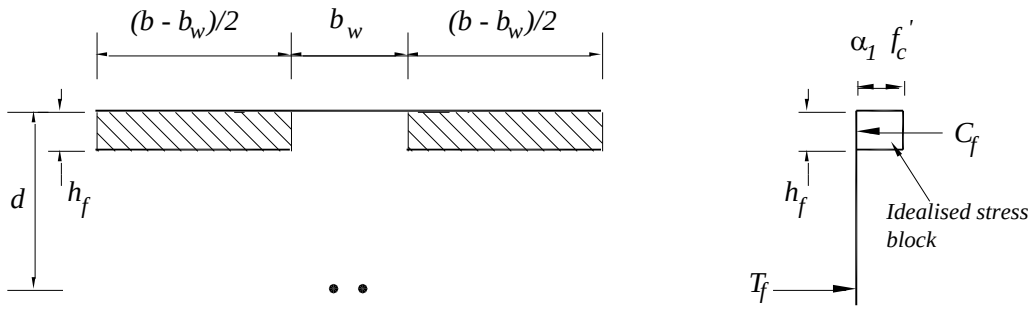

(d) Moment for stresses in the flange component

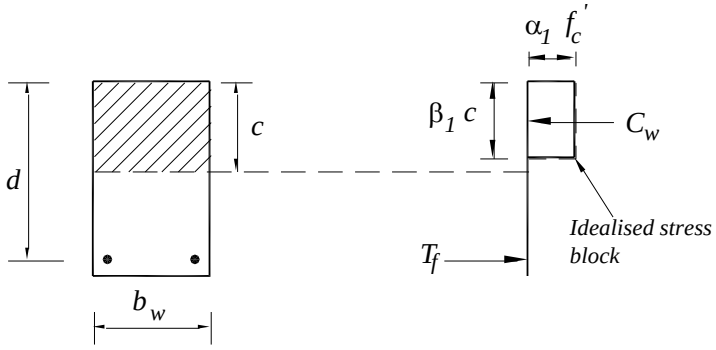

(e) Moment for stresses in the web component

Fig. 7: Strain and stress distributions of flanged section when neutral axis in the web.

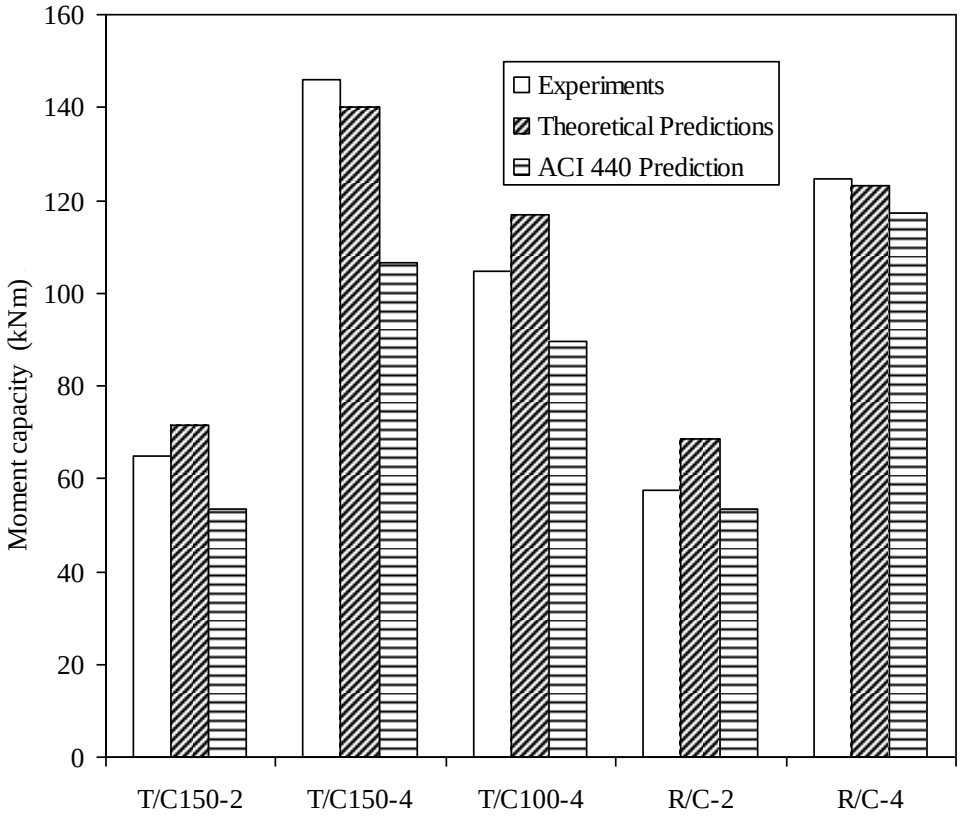

Fig. 8: Comparisons of moment capacity obtained from experiments, theoretical analysis and ACI 440 formula.

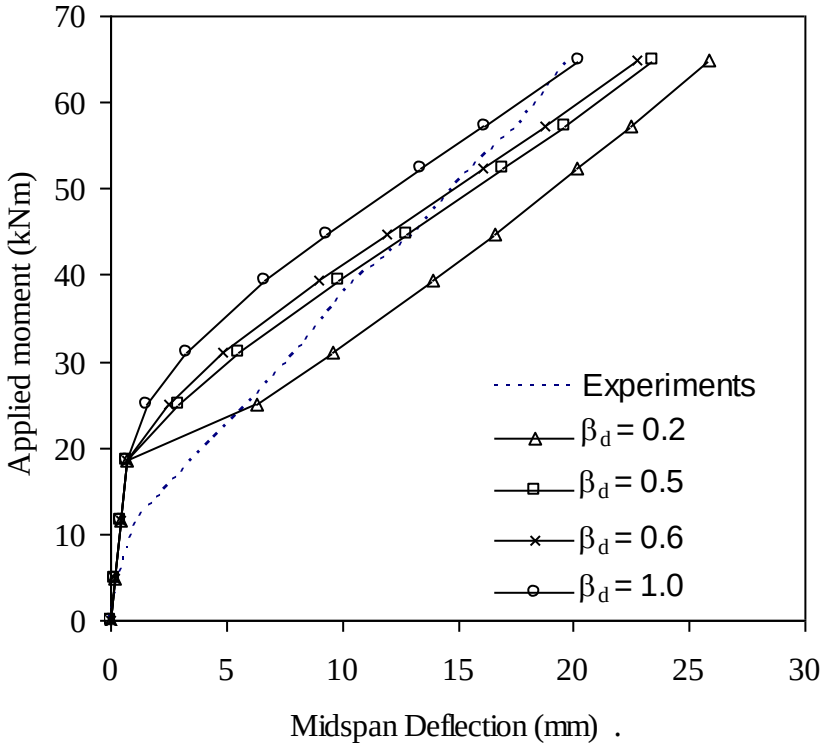

(a) T/C150-2

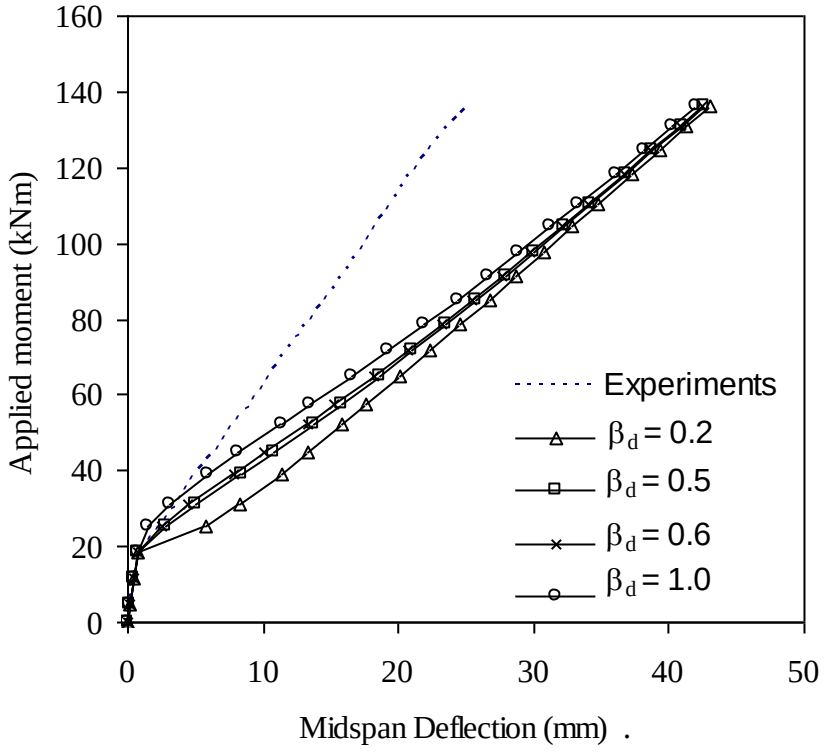

(b) T/C150-4

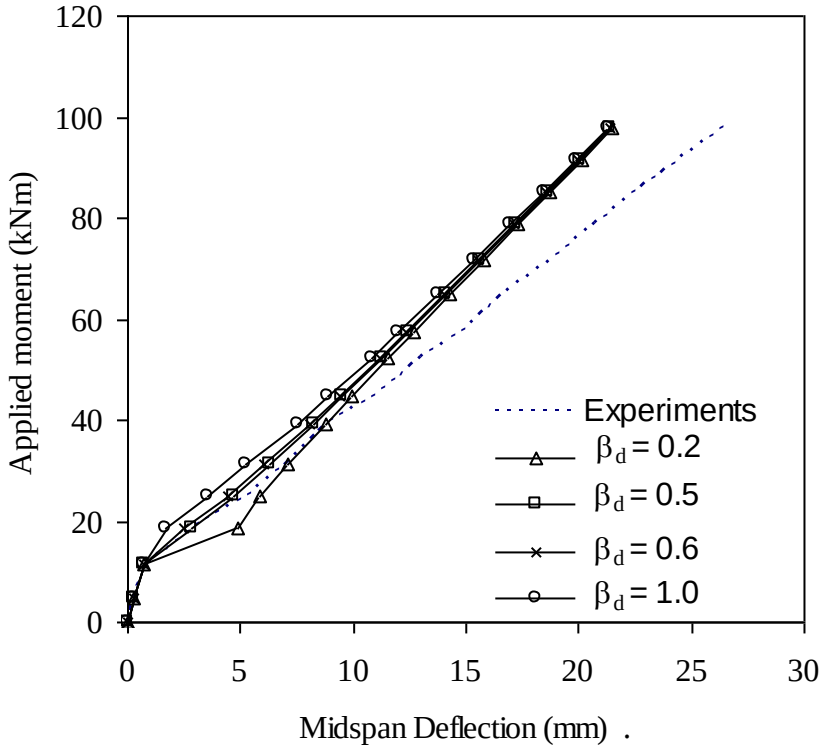

(c) T/C100-4

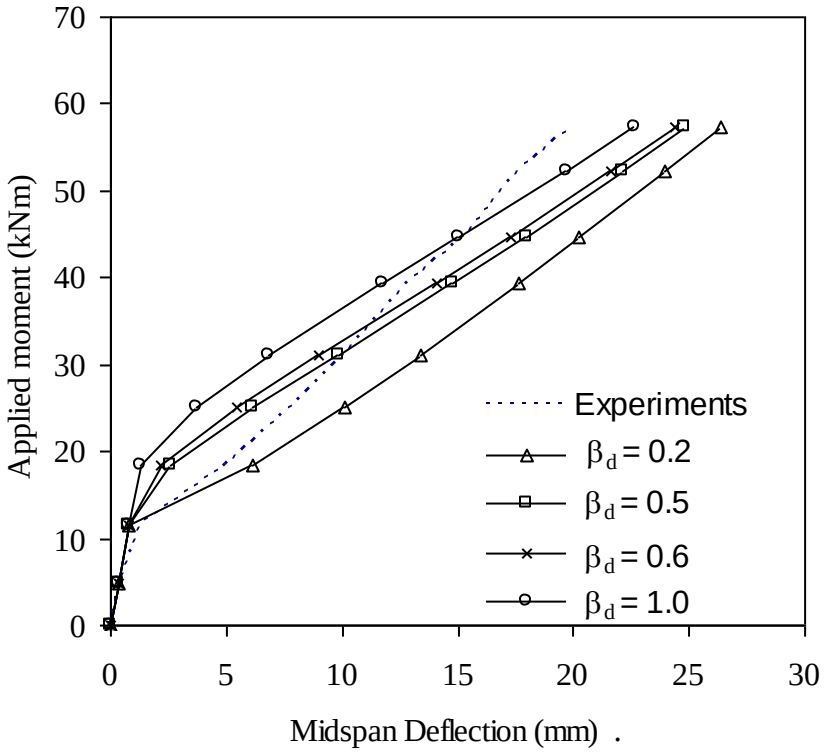

(d) R/C-2

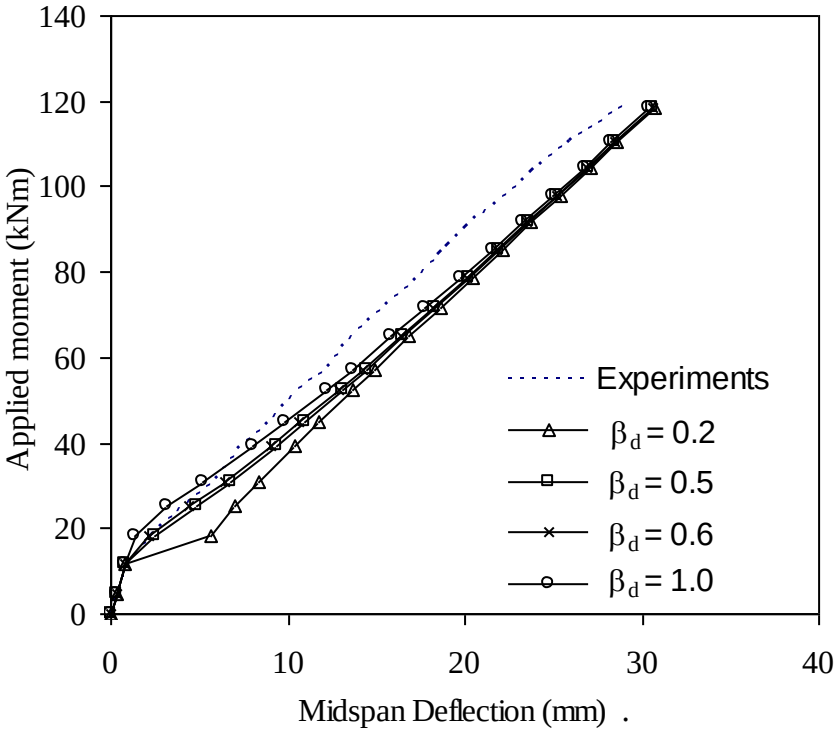

(e) R/C-4

Fig. 9: Comparisons of experimental mid-span deflection and ACI 440 prediction for different values of β_d.

Table 1: Geometrical and reinforcement details and test results of all beams tested.

Beam ID.	Overall depth (mm)	Flange thickness (mm)	Bottom reinforcement			Total top reinforcement			Concrete properties			First Cracking Load (kN)	Total Failure Load (kN)	Observed Mode of Failure
			Type	No. & dia.	area (mm²)	Type	No. & dia.	area (mm²)	f_{cu} (N/mm²)	f_t (N/mm²)	f_r (N/mm²)			
T/C150-2	350	150	CFRP	2#12mm	226	CFRP	6# 8mm	300	37.5	3.3	3.9	22	123.6	CFRP bar rupture
T/C150-4	350	150	CFRP	4#12mm	452	CFRP	6# 8mm	300	37.5	3.3	3.9	35	277.5	CFRP bar rupture
T/C100-4	300	100	CFRP	4#12mm	452	CFRP	6# 8mm	300	37.5	3.3	3.9	22	199.3	CFRP bar rupture
R/C-2	350	-	CFRP	2#12mm	226	CFRP	2# 8mm	100	40.5	3.6	4.3	22	109.2	CFRP bar rupture
R/C-4	350	-	CFRP	4#12mm	452	CFRP	2# 8mm	100	40.5	3.6	4.3	22	237.34	Concrete crushing
T/S150-3	350	150	Steel	3#16mm	603	Steel	6# 8mm	300	40.5	3.6	4.3	35	199.3	Yielding of steel bars

Table 2: Properties of steel and CFRP reinforcing bars.

	Yield strength (N/mm^2)	Ultimate tensile strength (N/mm^2)	Elastic modulus, (kN/mm^2)
8 mm dia. longitudinal steel bars	500	605	200
10 mm dia. steel stirrups	490	570	200
16 mm dia. longitudinal steel bars	510	615	200
8 mm dia. CFRP bars	N/A	1100	140
12 mm dia. CFRP bars	N/A	1060	200

Table 3: Strains and forces for balanced reinforcement case.

(a) Neutral axis in the flange

	Strains	Forces
Compression in concrete	$\varepsilon_c = 0.003$	$C_c = 0.85\beta_1 f_c^{'} b c_b$
Tension in FRP bars	$\varepsilon_f = \varepsilon_{fu}$	$T_f = A_{fb} f_{fu}$
Equilibrium Equations		$0.85\beta_1 f_c^{'} b c_b = A_{fb} f_{fu}$

(b) Neutral axis below the flange

		Strains	Forces
Compression in concrete	Flange	$\varepsilon_c = 0.003$	$C_f = 0.85 f_c^{'}\left(b - b_w\right) h_f$
	Web	$\varepsilon_c = 0.003$	$C_w = 0.85\beta_1 f_c^{'} b_w c_b$
Tension in FRP bars		$\varepsilon_f = \varepsilon_{fu}$	$T_f = A_{fb} f_{fu}$
Equilibrium Equations			$0.85 f_c^{'}\left(b - b_w\right) h_f + 0.85\beta_1 f_c^{'} b_w c_b = A_{fb} f_{fu}$

Table 4: Strains, forces and moments of flanged sections when neutral axis in the flange.

a) Concrete crushing failure mode

	Strains	Forces	Moments*
Compression in concrete	$\varepsilon_c = 0.003$	$C_c = 0.85\beta_1 f_c^{'} bc$	0
Tension in FRP bars	$\varepsilon_f = 0.003\frac{d-c}{c}$	$T_f = A_f f_f$	$A_f f_f \left(d - \frac{\beta_1 c}{2}\right)$
Equilibrium Equations		$0.85\beta_1 f_c^{'} bc = A_f f_f$	$M_n = A_f f_f \left(d - \frac{\beta_1 c}{2}\right)$
*moments are taken about the concrete compressive force.			

(b) FRP bar rupture failure mode

	Strains	Forces	Moments*
Compression in concrete	$\varepsilon_c = \varepsilon_{fu}\frac{c}{d-c}$	$C_c = \alpha_1\beta_1 f_c^{'} bc$	0
Tension in FRP bars	$\varepsilon_f = \varepsilon_{fu}$	$T_f = A_f f_{fu}$	$A_f f_{fu}(d - \frac{\beta_1 c}{2})$
Equilibrium Equations		$\alpha_1\beta_1 f_c^{'} bc = A_f f_{fu}$	$M_n = A_f f_{fu}(d - \frac{\beta_1 c}{2})$
*moments are taken about the concrete compressive force.			

Table 5: Strains, forces and moments of flanged sections when neutral axis below the flange.

(a) Concrete Crushing failure mode

		Strains	Forces	Moments*
Compression in concrete	Flange	$\varepsilon_c = 0.003$	$C_f = 0.85 f_c^{'}(b-b_w)h_f$	$0.85 f_c^{'}(b-b_w)(d-\frac{h_f}{2})h_f$
	Web	$\varepsilon_c = 0.003$	$C_w = 0.85\beta_1 f_c^{'} b_w c$	$0.85\beta_1 f_c^{'} b_w (d-\frac{\beta_1 c}{2})c$
Tension in FRP bars		$\varepsilon_f = 0.003\frac{d-c}{c}$	$T_f = A_f f_f$	0
Equilibrium Equations			$0.85 f_c^{'}(b-b_w)h_f + 0.85\beta_1 f_c^{'} b_w c = A_f f_f$	$M_n = 0.85 f_c^{'}(b-b_w)(d-\frac{h_f}{2})h_f + 0.85\beta_1 f_c^{'} b_w (d-\frac{\beta_1 c}{2})c$

*moments are taken about the level of FRP bars.

(b) FRP bar rupture failure mode

		Strains	Forces	Moments*
Compression in concrete	Flange	$\varepsilon_c = \varepsilon_{fu}\frac{c}{d-c}$	$C_f = \alpha_1 f_c^{'}(b-b_w)h_f$	$\alpha_1 f_c^{'}(b-b_w)(d-\frac{h_f}{2})h_f$
	Web	$\varepsilon_c = \varepsilon_{fu}\frac{c}{d-c}$	$C_w = \alpha_1\beta_1 f_c^{'} b_w c$	$\alpha_1\beta_1 f_c^{'} b_w (d-\frac{\beta_1 c}{2})c$
Tension in FRP bars		ε_{fu}	$T_f = A_f f_{fu}$	0
Equilibrium Equations			$\alpha_1 f_c^{'}(b-b_w)h_f + \alpha_1\beta_1 f_c^{'} b_w c = A_f f_{fu}$	$M_n = \alpha_1 f_c^{'}(b-b_w)(d-\frac{h_f}{2})h_f + \alpha_1\beta_1 f_c^{'} b_w (d-\frac{\beta_1 c}{2})c$

*moments are taken about the level of FRP bars.

Table 6: Theoretical predictions of moment capacity of the beams tested.

Beam Notations.	A_f (mm^2)	A_{fb} (mm^2)	c (mm)	M_{exp} (kNm)	M_{tho} (kNm)	M_{tho}/M_{exp}	Predicted failure mode
T/C150-2	226	1314.1	43.74	64.86	71.59	1.10	FRP bar rupture
T/C150-4	452	1314.1	61.58	145.87	139.97	0.96	FRP bar rupture
T/C100-4	452	1104.8	56.44	104.62	116.81	1.12	FRP bar rupture
R/C-2	226	399.8	77.88	57.33	68.41	1.19	FRP bar rupture
R/C-4	452	399.8	93.76	124.6	123.30	0.99	Concrete crushing

where A_f = area of CFRP bars, A_{fb} = area of CFRP bars at balanced failure, c = depth of neutral axis, M_{exp}= experimental moment capacity and M_{tho} = theoretical moment capacity. In the above table, it is assumed that $f_c^{'} = 0.85 f_{cu}$, where f_{cu} is the concrete cube compressive strength.

Table 7: Different values of β_d or α_b proposed in the literature.

Reference	α_b	β_d
Engel et al. [4]	0.1	0.2
Yost, Gross and Dienhart [11]	0.25	0.5
Theriault and Benmokrane [9] Masmoudi, Theriault and Benmakroni [7]	0.3	0.6
ACI committee 440 [3] Abdalla [1] Toutanji and Deng [10] Pecce, Manfredi and Cosenza [8]	0.5	1.0